Supplementary Material

Evidence for transmembrane H^+ transfer in a dihaem-containing membrane protein complex

M. G. Madej[1], H. R. Nasiri[2], N.S. Hilgendorff[1], H. Schwalbe[2], C. R. D. Lancaster[1*]

[1]Max Planck Institute of Biophysics, Dept. of Molecular Membrane Biology, Max-von-Laue-Str. 3, 60438 Frankfurt/M.,

[2]Institut für Organische Chemie und Chemische Biologie, Center for Biomolecular Resonance, Johann Wolfgang Goethe-Universität, Max-von-Laue-Str. 7, 60438 Frankfurt/M., Germany.

1. Supplementary Figures and Legends

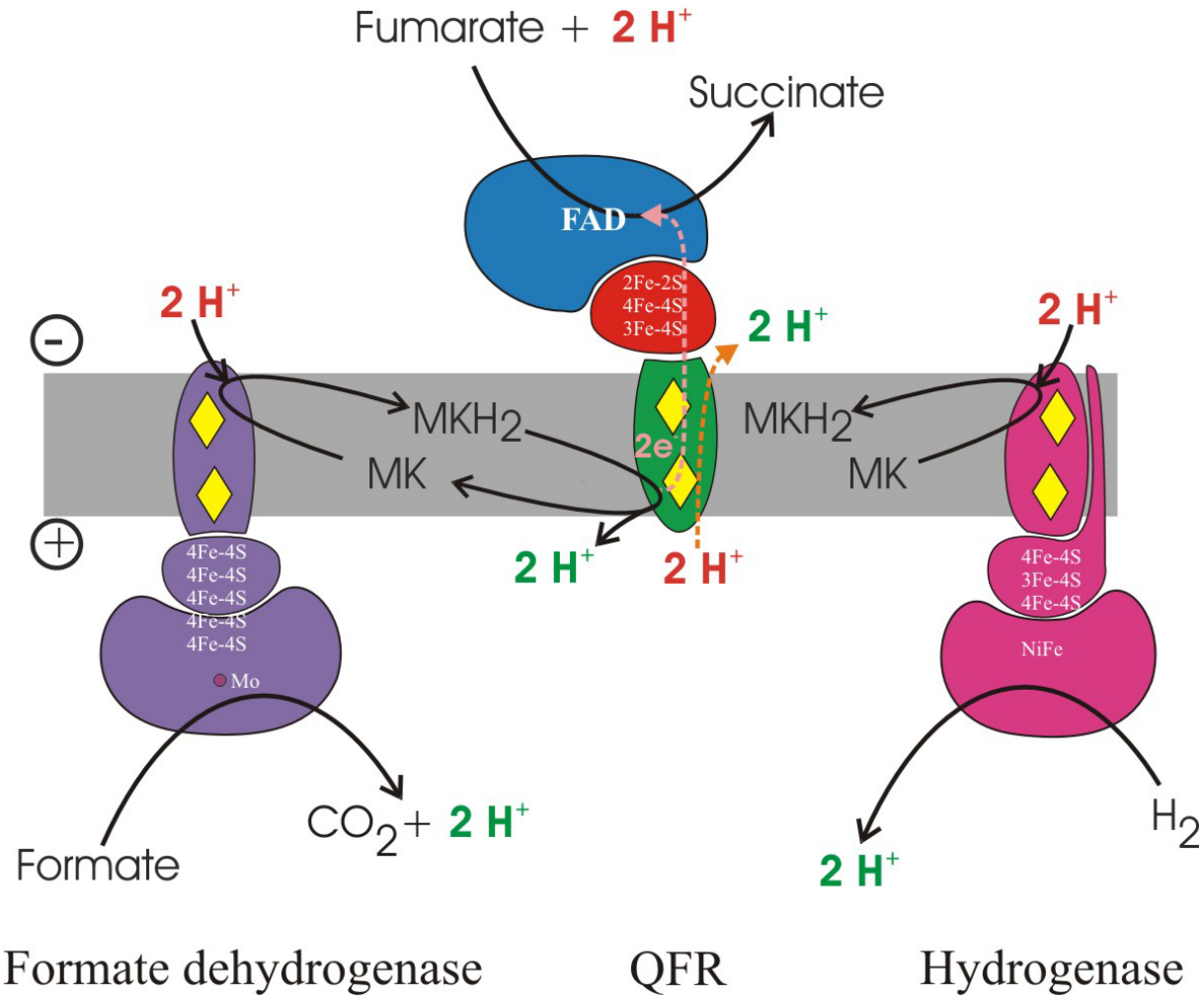

Figure S1. Electron and proton transfer in *W. succinogenes* fumarate respiration. Formate dehydrogenase is shown in purple, hydrogenase in pink. QFR subunits are colour-coded in blue (A subunit), red (B subunit) and green (C subunit). Haem groups are symbolised as yellow diamonds. Positive and negative sides of the membrane are the periplasm and the cytoplasm, respectively. Protons bound are shown in red, protons released in green.

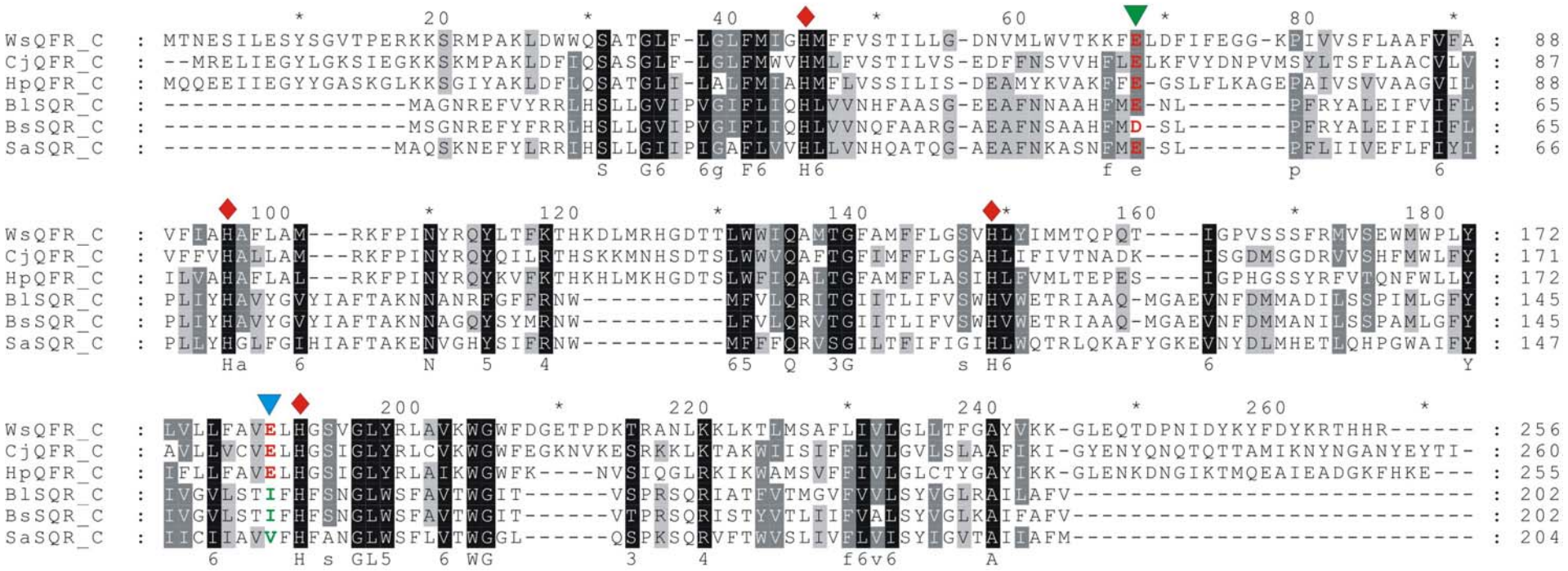

Figure S2. Sequence alignment. C-subunit sequence alignment of dihaem-containing succinate:menaquinone oxidoreductase enzymes from different species. QFR sequences from ε-proteobacteria (Ws: *W. succinogenes*, Cj: *C. jejuni*, Hp: *H. pylori*) and SQR sequences from Gram-positive bacteria (Bl: *B. licheniformis*, Bs: *B. subtilis*, Sa: *S. aureus*) were aligned with T-Coffee (Notredame *et al*, 2000) and viewed and edited using GeneDoc (Nicholas *et al*, 1997). Residues highlighted in black, dark grey and light grey are 100 %, 80 % and 60 % conserved respectively. The His ligands to the haem groups are indicated by red diamonds. The essential acidic constituent, labelled in red, of the menaquinol oxidation site is indicated with a green arrow. The most prominent acidic component of the E-pathway is indicated by a blue arrow. This residue is not conserved in SQRs, as labelled in green.

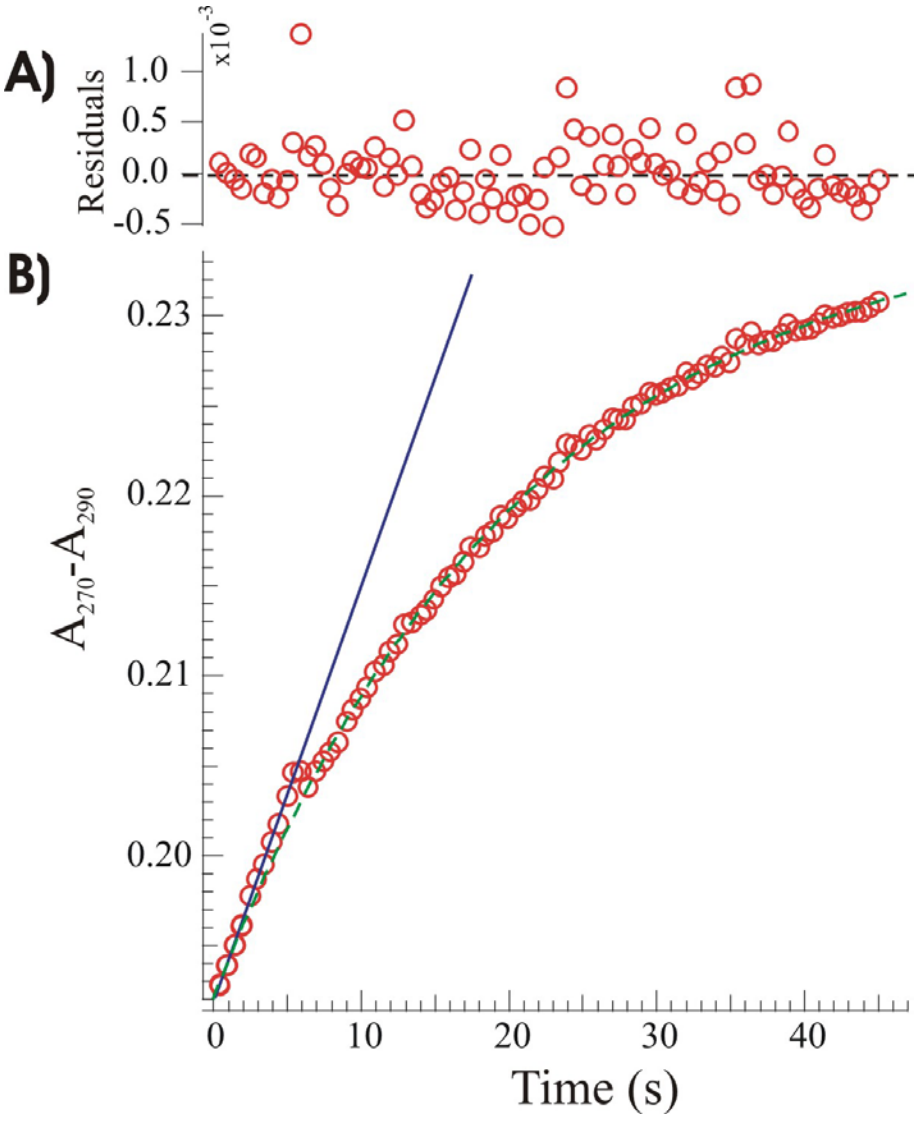

Figure S3. Enlargement of right half of Figure 1 C (after the addition of the uncoupler CCCP)
A) Residual plot for the fit in panel B.
B) Enlargement of right half of Figure 1 C (after the addition of the uncoupler CCCP). The data points $\Delta A(t)$ were fitted (blue) to the linear model equation S1 (see Supplementary Table SII; shown as blue line; points 0-22) and an exponential model equation S2 (shown as green dashed line; points 23-end).

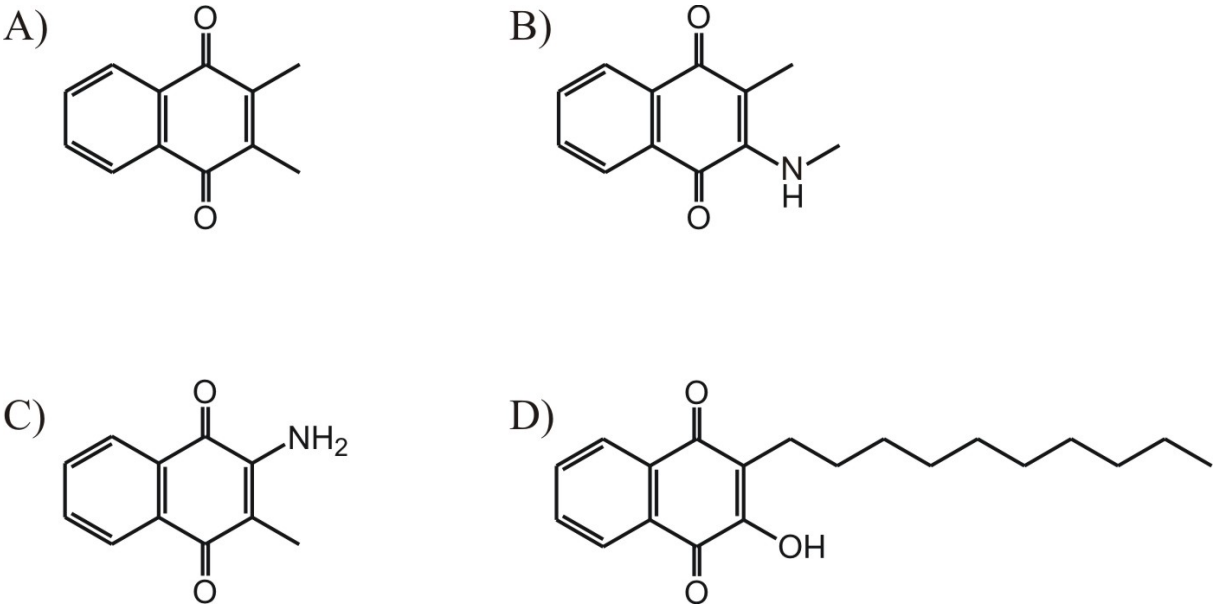

Figure S4. Chemical structures of synthesised naphthoquinones.

A) 2,3-Dimethyl-1,4-naphthoquinone (DMN)

B) 2-Methyl-3-methylamino-1,4-naphthoquinone (MMAN)

C) 2-Amino-3-methyl-1,4-naphthoquinone (AMN)

D) 2-Decyl-3-hydroxy-1,4-naphthoquinone (DHN)

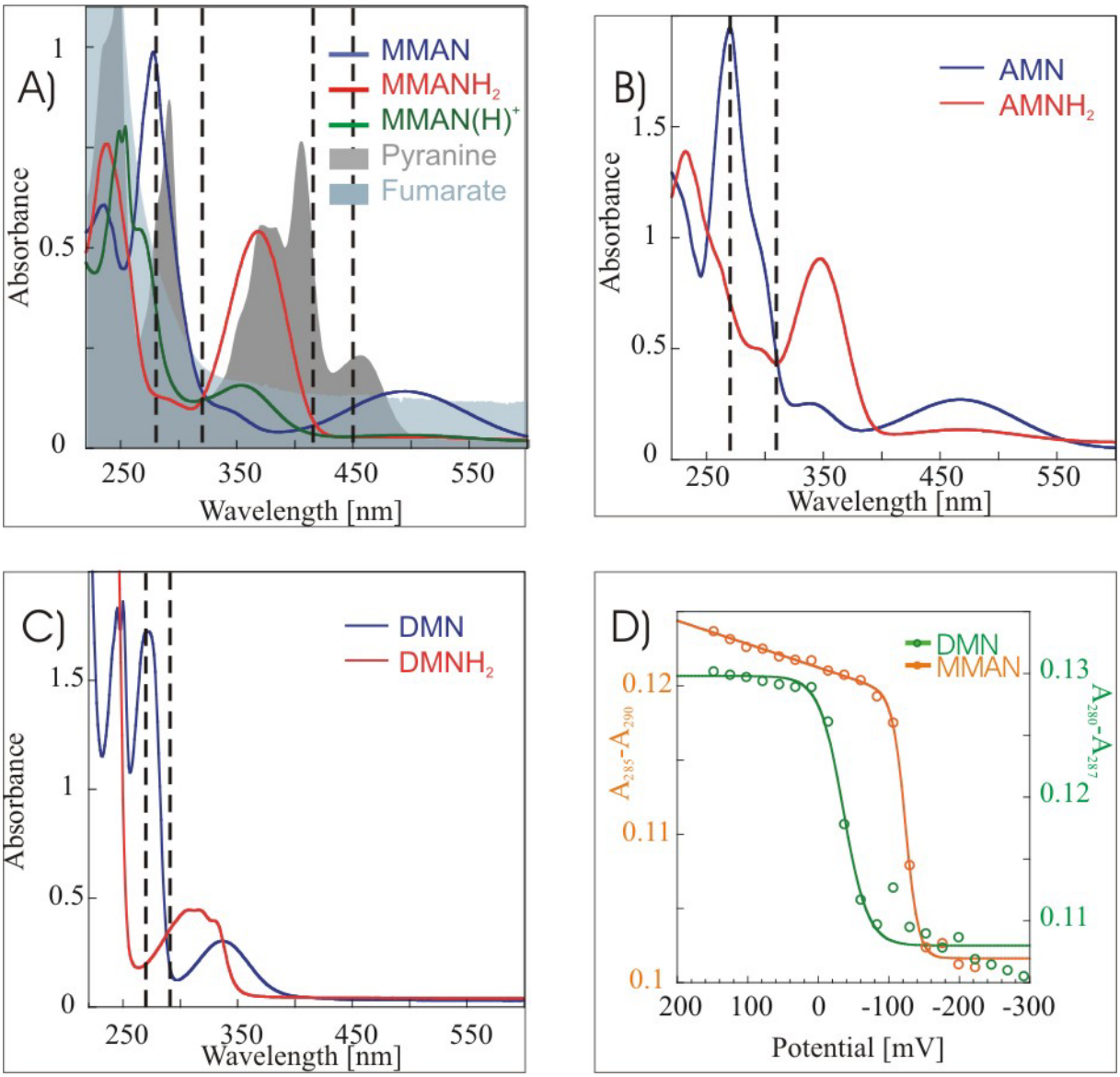

Figure S5. UV/VIS Spectra of oxidised and reduced quinones and *in situ* redox titration of DMN and MMAN

Spectra were recorded in 20 mM HEPES pH 7.5 buffer, the path length was 0.4 cm.
A) UV/VIS Spectra (recorded in H_2O) of MMAN (blue)/ $MMANH_2$ (red, reduced with solid $NaBH_4$, $\Delta\varepsilon_{280\text{-}320} = 27.6\ mM^{-1}cm^{-1}$) and other absorbance contributions in the pyranine/proteoliposome experiment shown in Figures 2A and 2B. UV/VIS Spectrum of $MMANH^+$ recorded in 36% HCl ($\Delta\varepsilon_{280\text{-}320}$ ($MMANH^+/MMANH_2$) = 5.8 $mM^{-1}cm^{-1}$). The pyranine absorbance is shown as grey area and fumarate absorbance is shown as transparent blue area. The spectra are scaled to the absorption of MMAN at λ 280 nm and shown in arbitrary units.
B) UV/VIS Spectra of AMN / $AMNH_2$ ($\Delta\varepsilon_{270\text{-}310} = 24.6\ mM^{-1}cm^{-1}$)
C) UV/VIS Spectra of DMN / $DMNH_2$ ($\Delta\varepsilon_{270\text{-}290} = 15.2\ mM^{-1}cm^{-1}$)
D) *In situ* redox titration of QFR-bound DMN ($\Delta\varepsilon_{280\text{-}287} = 9.9\ mM^{-1}cm^{-1}$) and MMAN ($\Delta\varepsilon_{285\text{-}290} = 5.0\ mM^{-1}cm^{-1}$).

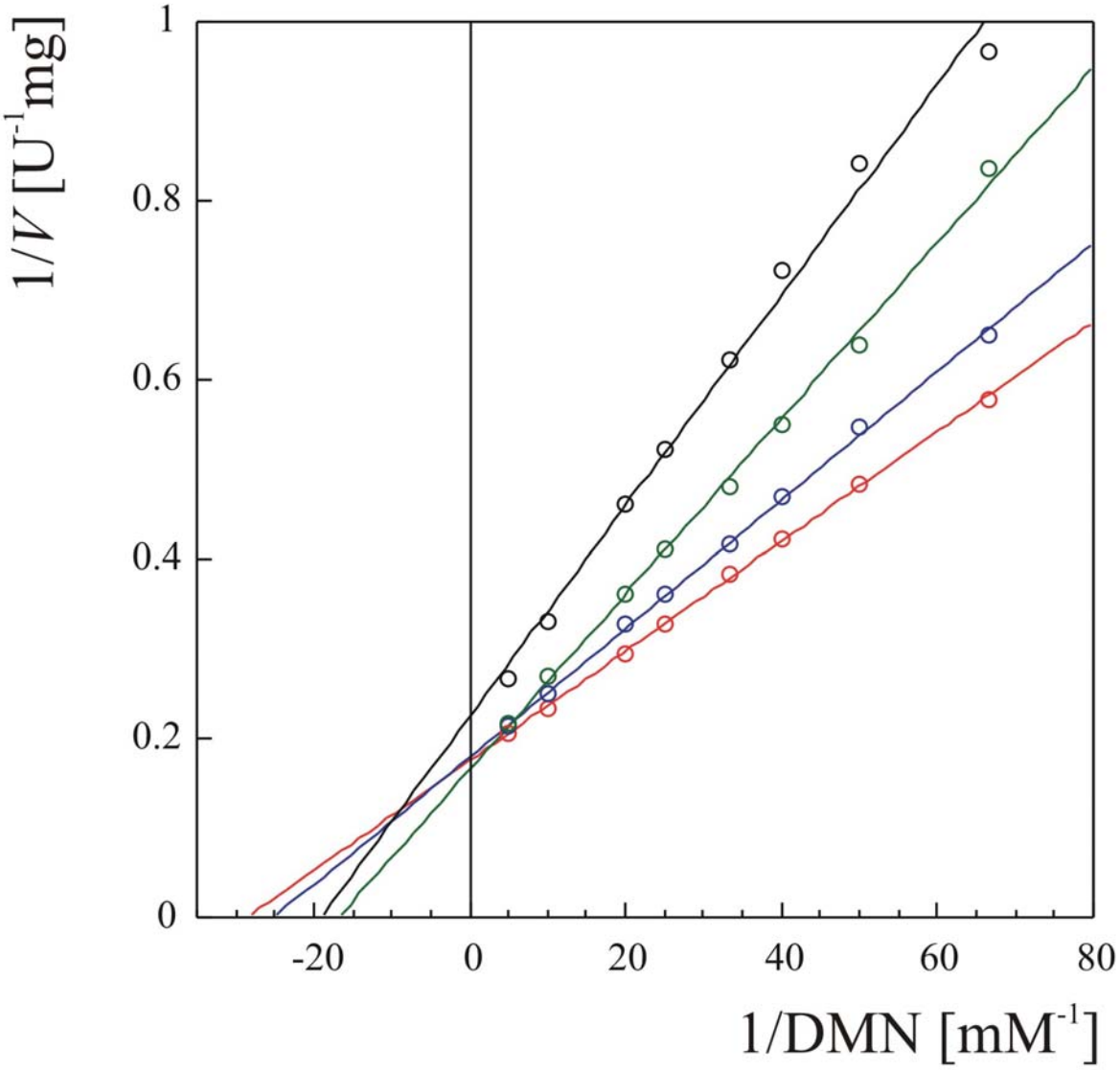

Figure S6. Double reciprocal plot of $DMNH_2$ oxidation by fumarate as catalysed by wild-type QFR from *W. succinogenes*, demonstrating the competitive nature of the inhibitor 2-decyl-3-hydroxy-1,4-naphthoquinone (DHN). The specific activities were determined as described in the absence of DHN (red) and in the presence of 1 μM (blue) 2 μM (green), and 4 μM DHN (black), respectively.

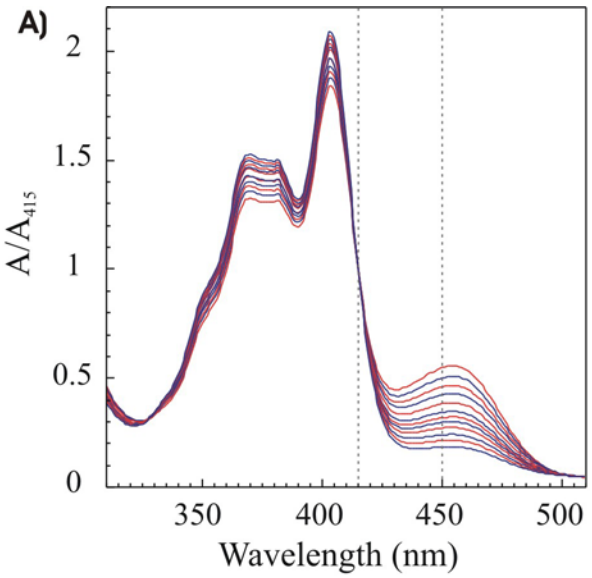

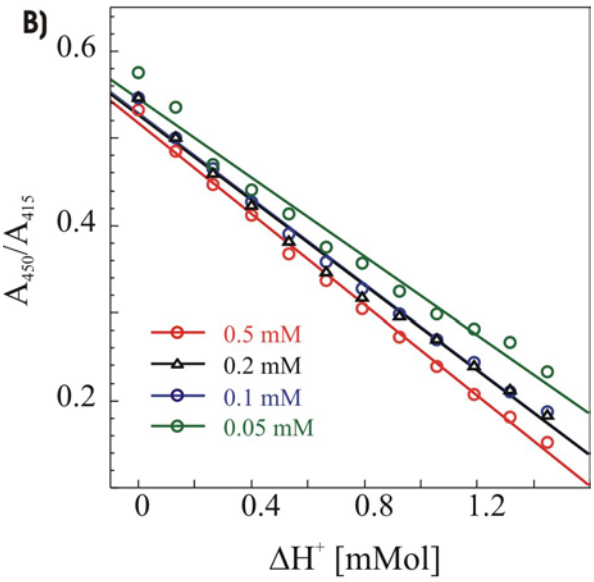

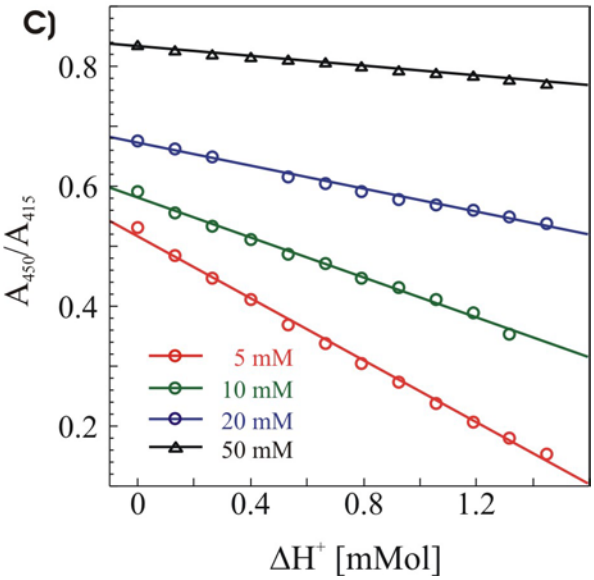

Figure S7. Titration of pyranine. **A)** Normalised UV-Vis spectra of pyranine (A/A_{415}) upon addition of HCl. (5 mM HEPES, 0.2 mM pyranine, addition of 1µl 120 mM HCl per step). The isosbestic point (λ = 415 nm) and the indicator wavelength (λ = 450 nm) are indicated by dashed lines. The normalization of the spectra followed the same procedure as in Figure 2B, by division by the isosbestic point (IP_{415}) at λ=415 nm.

B) The dependence of the absorbance ratio of A_{450}/A_{415} on added HCl at constant buffer concentration, varying the pyranine concentration. (5 mM HEPES, pyranine concentration as indicated in the plot inset) The normalized and averaged slope is 0.243 $mM_{H^+}^{-1}$ at 5 mM HEPES. **C)** The dependence of the absorbance ratio of A_{450}/A_{415} on added HCl at constant pyranine concentration, varying buffer concentration. (HEPES concentration as indicated in the plot inset, 0.5 mM pyranine). The normalized slopes are: 0.259 $mM_{H^+}^{-1}$ at 5 mM HEPES, 0.166 $mM_{H^+}^{-1}$ at 10 mM HEPES, 0.096 $mM_{H^+}^{-1}$ at 20 mM HEPES, 0.041 $mM_{H^+}^{-1}$ at 50 mM HEPES.

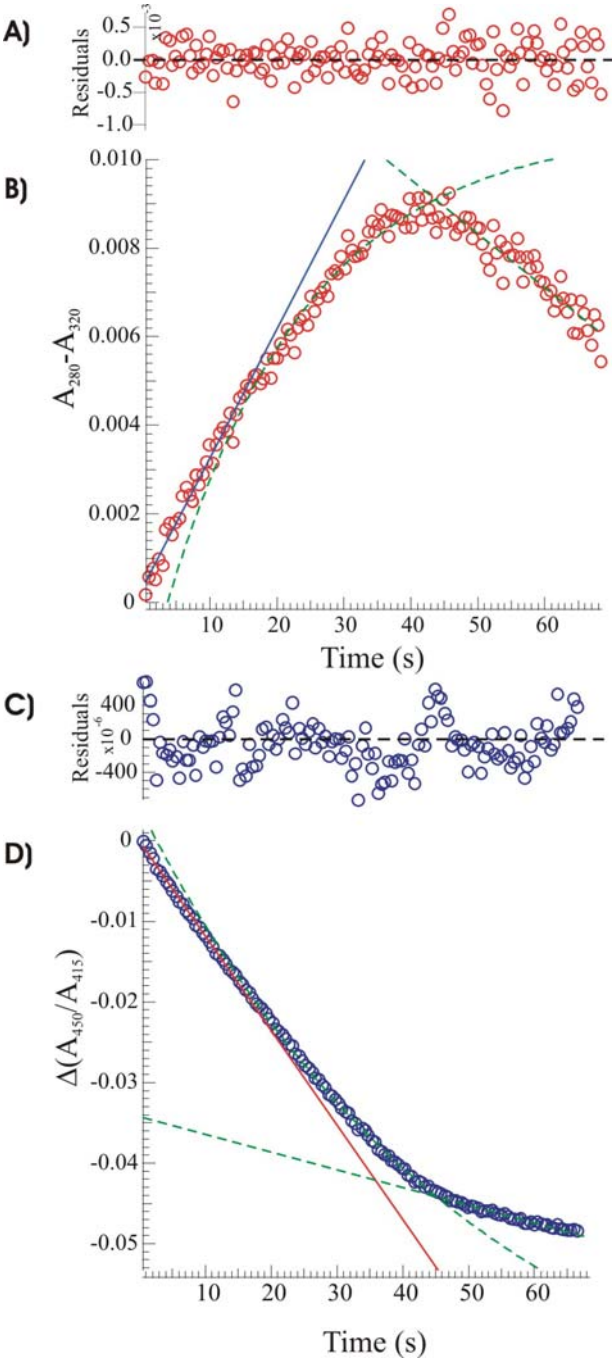

Figure S8. Curve fitting of Figures 2A and B

A) Residual plot for the fit in panel B.

B) Apparent progress curve of $MMANH_2$ oxidation by proteoliposomal E180Q-QFR taken from Fig.2 A and fitted to linear model equation S1 (see Table SII; shown as blue line; points 0-28), exponential model equation S2 (shown as green dashed line; points 29-87) and linear model equation S1 (shown as green dashed line; points 88-135).

C) Residual plot for the fit in panel D.

D) Progress curve of the acidification of the interior of the proteoliposomes upon $MMANH_2$ oxidation by proteoliposomal E180Q-QFR taken from Fig.2 B and fitted accordingly to panel B. Linear model S1 (see Table SII; shown as red line; points 0-28), exponential model S2 (shown as green dashed line; points 29-87) and linear model S1 (shown as green dashed line; points 88-end).

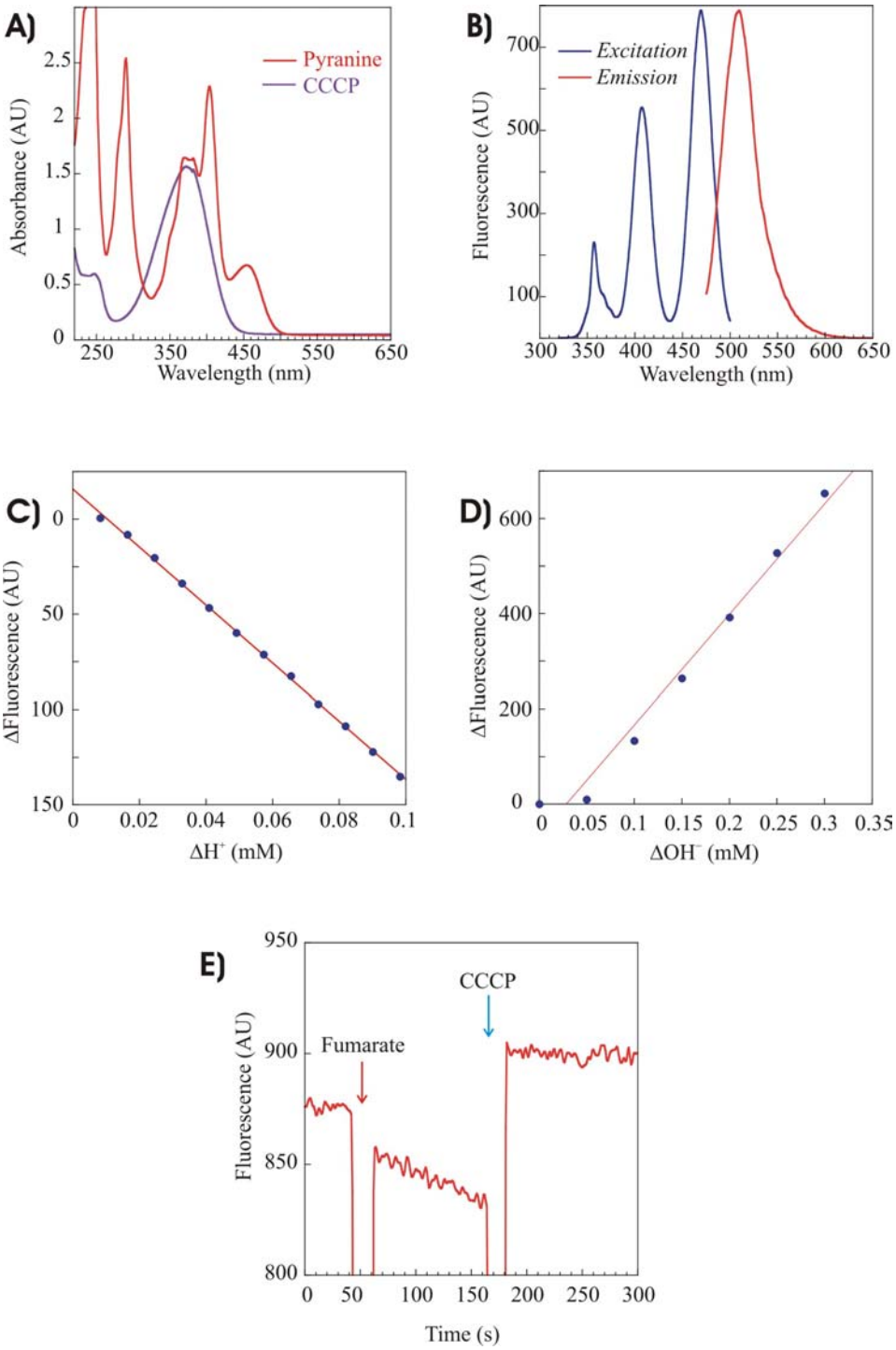

Figure S9. Spectroscopic composition of pyranine fluorescence measurements
A) Superposition of the UV/Vis absorption spectra of pyranine (red) and CCCP (purple). **B)** Excitation and emission spectra of pyranine (3 µM) in HEPES buffer (pH 7.3) were recorded in 1×0.4 cm quartz cells, slits: 2.5 nm × 3.5 nm. Excitation was monitored with respect to λ_{em}= 510 nm. Emission spectrum taken at λ_{exc}=470nm. **C)** Titration of the liposomes with HCl. **D)** Titration of the liposomes with NaOH. **E)** Fluorescence monitoring of the acidification of the interior of proteoliposomes with reconstituted E180Q QFR catalysing $MMANH_2$ oxidation by fumarate. The reaction was started by the addition of 20 µM fumarate (red arrow); the protonophore CCCP was added subsequently (blue arrow). Reaction conditions same as Fig. 2 A + B. λ_{exc}=470nm, λ_{em}= 510 nm, slits: 2.5 nm×4.0 nm.

2. Supplementary Methods

2.1. Synthesis of naphthoquinones.

General Remarks. NMR spectra were recorded on spectrometers operating at a ^{1}H frequency of 250 MHz. Elementary analyses were measured on a Foss Heraeus CHIN-O-RAPID instrument. IR spectra were recorded on a PERKLIN ELMER spectrometer. Low resolution electronspray mass spectra (ESI) were recorded on a Fisons VG Platform II spectrometer. All reactions were monitored by thin-layer chromatography (TLC), performed on silica gel POLYgram® (Macherey-Nagel). Chromatographic purifications were done with Merck silica gel 60.

Synthesis of 2,3-Dimethyl-1,4-naphthoquinone (DMN). DMN was synthesized following literature procedures (Wurm and Geres, 1984) as described earlier (Lancaster *et al*, 2005). The crude product was purified by silica chromatography (chloroform:cyclohexane 10:1), Rf = 0.46.

^{1}H-NMR (250.13 MHz, $CDCl_3$): δ [ppm]= 8.2 – 7.95 (m, 2H, aromatic protons), 7.65 – 7.58 (m, 2H, aromatic protons), 2.09 (s, 6H, CH_3).

^{13}C-NMR (62.9 MHz, $CDCl_3$): δ [ppm]= 184.9 (C=O), 143.4 (C), 133.3 (CH), 132.1 (C), 126.2 (CH), 12.9 (CH_3).

IR (KBr pellet): 1659.45;1592.91;1372.10;1295.93;790.67;699.07 cm^{-1}.

Anal.calcd for $C_{12}H_{10}O_2$: C 77.4, H 5.41; Found: C 77.28, H 5.49

E_0= -870 mV (in dimethoxyethane/tetrabutylammoniumperchlorat on platinum working and counter electrodes. potential is quoted vs. Ag/AgCl reference electrode, sweep rate 50 mV/s), 20 mV lower than K2.

Synthesis of 2-Methyl-3-methylamino-1,4-naphthoquinone (MMAN). MMAN was synthesized following literature procedures (Ohta *et al*, 1994). The crude product was purified by silica chromatography (CH_2Cl_2); Rf = 0.53.

^{1}H-NMR (250.13 MHz, $CDCl_3$): δ[ppm]= 8.2 – 7.8 (m, 2H, aromatic protons), 7.7 – 7.4 (m, 2H, aromatic protons), 5.7 (s br,1H, NH), 3.15 (s, 3H, NH*CH₃*), 2.19 (s, 3H, CH_3).

^{13}C-NMR (62.9 MHz, $CDCl_3$): δ[ppm]= 183.0; 182.0 (C=O), 146.9; 133.5; 130.2; 111.9 (C), 134.3; 131.7; 126.1; 125.9 (CH), 32.8; 10.9 (CH_3).

IR(KBr pellet): 3366.14;1669.09;1599.66;1563.02;1519.63;1343.18;1283.39 and 728.96 cm^{-1}.

MS (ESI): m/z: 201.8 M^+

Anal.calcd. for $C_{12}H_{11}NO_2$: C 71.63, H 5.51, N 6.96; Found: C 71.82, H 5.26, N 6.92.

E_0= -930 mV (in dimethoxyethane/tetrabutylamoniumperchlorat on platinum working and counter electrodes. potential is quoted vs. Ag/AgCl reference electrode, sweep rate 50 mV/s), 80 mV lower than K2.

.

2-Amino-3-methyl-1,4-naphthoquinone (AMN). AMN was synthesized by a nitration/reduction sequence from 2-methyl-1,4-naphthoquinone. The nitration (Boyle *et al*, 1984) was carried out using a (1:1) mixture of concentrated HNO_3 and concentrated H_2SO_4 heated to 60°C:

2-Nitro-3-methyl-1,4-naphthoquinone: ^{1}H-NMR (250.13 MHz, $CDCl_3$): δ[ppm]= 8.1 – 8.0 (m, 2H, aromatic protons), 7.8 – 7.7 (m, 2H, aromatic protons), 2.1 (s, 3H, CH_3).

^{13}C-NMR (62.9 MHz, $CDCl_3$): δ[ppm]=183.5 (C=O), 175.1 (CNO_2), 137.0; 131.3; 130.0 (C), 135.1;134.9;127.3;127.0 (CH), 11.8 (CH_3).

Anal.calcd for $C_{12}H_7NO_4$: C 60.83, H 3.25, N 6.45; Found: C 60.62, H 3.39, N 6.30.

The reduction of the resulting 2-nitro-3-methyl-1,4-naphtoquinone gave the desired product. To a suspension of 0.1 g (0,46 mmol) of 2-nitro-3-methyl-1,4-naphthoquinone in 1.3 ml water 0.26g (1,48 mmol) sodium hydrosulfite was added; the reaction was refluxed for 2h. After cooling to room temperture, the precipitate was filtered and dried to give 0.083 g (97%) pure amine as a red powder.

^{1}H-NMR (250.13 MHz, $CDCl_3$): δ[ppm]= 8.0 – 7.9 (m, 2H, aromatic protons), 7.6 – 7.4 (m, 2H, aromatic protons), 4.8 (s, br, 2H, NH_2), 1.94 (s, 3H, CH_3).

^{13}C-NMR (62.9 MHz, $CDCl_3$): δ [ppm]=182.9; 181.2 (C=O), 145.3; 133.2; 130.4; 113.2 (C), 134.2, 132.0, 126.2, 125.8 (CH), 9.2 (CH_3).

IR (KBr pellet) 3643.84;3460.63;3351.68;1676.8;1614.13;1582.31;1359.57;723.18 cm^{-1}.

E_0= -900 mV (in Dimethoxyethane/tetrabutylammoniumperchlorat on platinum working and counter electrodes. potential is quoted vs. Ag/AgCl reference electrode, sweep rate 50 mV/s) 50 mV lower than K2.

MS (ESI): m/z: 187.7 M^+

2-decyl-3-hydroxy-1,4-naphthoquinone. 2-decyl-3-hydroxy-1,4-naphthoquinone was synthesized by an alkylation/epoxidation and acid catalyzed epoxide cleavage of 1,4-naphthoquinone. The decyl side chain was introduced by a radical Hundsdiecker decarboxylation of undecanoic acid using silver nitrate and peroxydisulfate. A mixture of 1,4-

naphthoquinone 2 g (12,6 mmol), undecanoic acid 2,8 g (15,1 mmol) and silver nitrate 0,5 g (2,9 mmol) in 60 ml acetonitrile/water mixture (5:1) was heated at 80°C, at this temperature a solution of 5.7 g (25 mmol) ammonium persulfate in 20 ml water was slowly added. After 2h, the mixture was diluted with water and extracted twice with dichloromethane, dried and concentrated under reduced pressure. The crude product was purified by silica chromatography (hexane:ethylacetate 4:1) to give 0.695 g (18,5 %) of 2- decyl-1,4-naphthoquinone.

Rf =0.5,^{1}H-NMR (250.13 MHz, $CDCl_3$):
δ= 8.1 – 8.0 (m, 2H, aromatic protons), 7.8 – 7.7 (m, 2H, aromatic protons), 6.8 (s, 1H, CH), 2.6 (t, *J* = 7.8 Hz, 2H, CH_2), 1.6 – 1.2 (m, 16H, CH_2), 0.9 (t, *J* = 6,5 Hz, 3H, CH_3).
^{13}C-NMR (62.9 MHz, $CDCl_3$) δ=185.2 (C=O), 152.0; 132.3; 132.1(C), 134.7; 133.6; 126.6; 126.0 (CH), 31.8; 29.5; 29.5; 29.4; 29.3; 28.0, 22.6 (CH_2), 14.1 (CH_3).
IR(KBr pellet): 2917.77;2851.24;1664.27;1621.84;1592.91;1335.46;1305.57;1256.40;930.49 and 781.99 cm^{-1}.
Anal.Calcd. for $C_{20}H_{26}O_3$: C 80.5, H 8.78; Found: C 80.25, H 8,76.

In the second step, 2- decyl-1,4-naphthoquinone was converted to 1a-decyl-1a, 7a Dihydro-naphth[2,3b]oxirene-2,7-dione via Δ^2 epoxidation. 0.322 g (1.07 mmol) of 2- decyl-1,4-naphthoquinone was dissolved in ethanol (1 ml), a solution of alkaline hydrogen peroxide (0.5 ml of 30% H_2O_2, 20 mg sodium carbonate in 0.2 ml water) was added. After 1h stirring at room temperature, it was diluted with water and extracted twice with dichloromethane, dried and concentrated under reduced pressure to give 0.28g (90%) of the epoxide.
2-decyl-1a, 7a Dihydro-naphth[2,3b]oxirene-2,7-dione
Rf =0.6 (hexane:ethylacetate 6:1).
^{1}H-NMR (250.13 MHz, $CDCl_3$): δ [ppm]= 8.0 – 7.9 (m, 2H, aromatic protons), 7.8 – 7.7 (m, 2H, aromatic protons), 3.8 (s, 1H, CH), 2.3 – 2.2 (m, 1H, CH_2), 1.9 – 1.8 (m, 1H, CH_2), 1.5 – 1.4 (m, 16H, CH_2), 0.9 (t, *J* = 6,5 Hz, 3H, CH_3).
^{13}C-NMR (62.9 MHz, $CDCl_3$): δ [ppm]=192.0 ; 191.7 (C=O), 132.4; 131.8; 64.0 (C), 134.5; 134.2; 127.4; 126.7; 60.1 (CH), 31.8; 29.6; 29.5; 29.4; 29.3;29.3; 28.2; 24.4; 22.6 (CH_2), 14.1 (CH_3).

In the last step, the epoxide was cleaved under acetic condition to give the desired product. 0.250 g (0.79 mmol) epoxide was dissolved in 1 ml concentrated sulfuric acid and stirred at

room temperature for 10 min. It was diluted in water and extracted twice with dichloromethane, dried and concentrated under reduced pressure. The crude product was purified by silica chromatography (hexane:ethylacetate 6:1) to give 0.121 g (49 %) of 2-decyl-3-hydroxy-1,4-naphthoquinone; Rf =0.5 (hexane:ethylacetate 6:1).

^{1}H-NMR (250.13 MHz, $CDCl_3$): δ [ppm]= 8.0 – 7.9 (m, 2H, Aromat), 7.7 – 7.5 (m, 2H, Aromat), 7.2 (s, 1H, OH), 2.5 – 2.4 (t, 2H, CH_2), 1.5 – 1.2 (m, 16H, CH_2), 0.7 (t, J = 6,5 Hz, 3H, CH_3).

^{13}C-NMR (62.9 MHz, $CDCl_3$): δ [ppm]=184.3 ; 181.4 (C=O), 153.0; 132.9; 129.4; 124.8 (C), 134.8; 132.8; 126.7; 126.0 (CH), 31.9; 29.8; 29.6; 29.5; 29.4; 29.3; 28.3; 23.4; 22.6 (CH_2), 14.1 (CH_3).

IR(KBr pellet): 3366.14;2916.81;2852.2;1663.3;1640.16;1591.95;1347.03;1267.00;1213.97 and 722.21 cm^{-1}.

Anal.Calcd. for $C_{20}H_{26}O_3$: C 76.4, H 8.3; Found: C 75.12, H 8,20.

2.2. *In situ* redox titration of QFR-bound naphthoquinones

Equimolar amounts (3 µM) of *W. succinogenes* QFR and DMN were added to 950 µl N_2-flushed 20 mM HEPES buffer, pH 7.3. Sodium dithionite (30 mM in 1 M HEPES buffer, pH 7.3) was added in 1 µl increments. The solution was equilibrated for 90 s under an argon atmosphere. UV-Vis spectra were recorded from 650 nm to 230 nm. DMN and MMAN reduction were monitored by calculating the absorption differences ΔA_{280}-A_{287} and ΔA_{290}-A_{295}, respectively.

2.3. Calibration of pyranine titration

The spectra used for calculation of the acidification of the proteoliposome interior were normalized to the isosbestic point (IP_{415}) at λ = 415 nm, Fig. S7A). This method is based on the representation of absorbance change as the ratio of the absorbance at IP_{415} (A_{415}) to the absorbance at the indicator wavelength (A_{450}), Fig. S7B, C). Unlike the absorbance at the indicator wavelength, the absorbance at IP_{415} is independent of the H^+ concentration. The ΔpH (= $\log_{10}((\Delta c[H^+]\cdot V_i)/10^{-7.5})$ with $\Delta c[H^+]$=Δ (A450/A415)/0.243)) was calculated from the amplitude of the pyranine signal using the conversion factor of 0.243 $mM_{H^+}^{-1}$. (see Figure S7B). The proteoliposome exterior is buffered with 50 mM HEPES so that all the signal is contributed from the proteoliposomal interior.

The calibration of the entrapped pyranine fluorescence (Figure S9) as a function of pH was performed by diluting pyranine loaded vesicles in buffer directly in a fluorescence cuvette.

The liposomes were then permeabilized to protons through the addition of 12 µM CCCP to the medium. Valinomycin was added to sustain the ionic strength. The presence of the ionophore certified that the pH inside and outside the vesicles were balanced throughout the entire experiment. After adding small aliquots of 0.1 M NaOH or 0.1 M HCl to the fluorescence intensity was measured (Figures S9 C and D).

2.4 Determination of the H^+/e^- ratio

The H^+/e^- ratio was calculated from the ratio of the turnover rates in the steady-state phase (ΔA_c) of the $MMANH_2$ oxidation and the acidification of the proteosomal interior (Tab.SII).

3. Supplementary Tables

Table SI. Data collection and refinement statistics

Data set		
X-ray source	ESRF (Grenoble) ID14-3 / ID14-1	
Wavelength [Å]	0.931 / 0.934	
Space group	$P2_1$	
Unit cell parameters [Å]	a= 85.1 b = 188.8 c = 117.8 β = 104.5°	
Resolution* [Å]	28.75 – 1.78	(1.84-1.78)
Unique reflections*	317,968	(23,725)
R_{sym} *	0.098	(0.346)
Completeness* [%]	92.3	(69.0)
<I/sig(I)>*	16.5	(3.0)
Redundancy*	3.8	(2.6)
Refinement		
Resolution*	28.70 – 1.78	(1.82 – 1.78)
R_{cryst}*	0.229	(0.360)
R_{free}*	0.237	(0.375)
Protein non-hydrogen atoms	18,295	
Heterogen non-hydrogen atoms	404	
Solvent non-hydrogen atoms	990	
B values		
From Wilson plot [$Å^2$]	23.2	
Mean B value [$Å^2$]	38.8	
Coordinate error from cross-validated Luzzati plot [Å]		0.24
R.m.s deviations		
Bond lengths [Å]	0.007	
Bond angles [°]	1.3	
Dihedral angles [°]	21.2	
Improper angles	1.65	

* Values in parentheses apply to highest resolution shell.

Table SII. Rate constants as obtained from the respective fit to the kinetic models indicated.

Table SII

Experiment	Figure:	ΔA_c ($\mu mol \cdot s^{-1}$)	k_{app} ($\mu mol \cdot s^{-1}$)	ΔA_c* ($\mu mol \cdot s^{-1}$)
$DMNH_2$ Oxidation in the absence of CCCP	1C left 1D	9.7e-03 ± 9.6e-04	-	<<0.01
$DMNH_2$ Oxidation in the presence of CCCP	1C right S3	36.28 ± 0.052	7.39 ± 0.136	-
$MMANH_2$ Oxidation	2A	20.00 ± 0.007	32.40 ± 5.016	-8.43 ± 0.005
Pyranine signal upon $MMANH_2$ oxidation	2B	-40.64 ± 0.049	-679.40 ± 0.095	-7.69 ± 2.1e-5
H^+/e^-		2.03 ± 0.056	-	-

$$S \xrightarrow{k_1} P \xrightarrow{k_2} P'$$

S: $MMANH_2$; *P*: MMAN; *P*': $MMANH^+$

$$A(t) = A_0 + \Delta A_c t \quad \text{(S1)}$$

$$A(t) = A_0 + A_1 \cdot e^{(-k_{app} \cdot t)} \quad \text{(S2)}$$

A_0: extrapolated initial absorbance, $A(t)$: absorbance after time t, t: time, ΔA_c: constant slope in steady-state , ΔA_c*: second linear phase if reaction linear biphasic, k_{app}: apparent rate constant of the exponential process.

4. Supplementary Discussion

Closer inspection of the $DMNH_2$ oxidation trace in Figure 1C recorded on the variant enzyme E180Q before the addition of CCCP reveals a slightly positive initial slope in the first 15 to 20 seconds of the reaction (Figure 1D). Assuming a proteoliposomal internal volume of 1.75 µl, this initial slope corresponds to 0.23 µmol of $DMNH_2$ oxidised. Taking into account an H^+/e^- ratio of 1.0 (Table I), we calculate that 0.46 µmol H^+ were transferred into the proteoliposomes, which corresponds to a reduction in pH of 1.03 pH units. This inferred build-up of a transmembrane Δp appears to be sufficient to slow down the reaction, so that after 20 seconds, no further oxidation of $DMNH_2$ is observed.

After the CCCP addition the thermodynamic control is released. The progress curve of $DMNH_2$ oxidation in Figure S3B can be fitted disjointly to equations S1 and S2 (Table SII) which includes a linear and an exponential term. The linear term describes the Michaelis-Menten behavior; the exponential phase is very likely caused by the product accumulated in the vesicles which competes for the active site. These effects of product inhibition are currently under investigation.

The progress curves of $MMANH_2$ oxidation by fumarate as catalysed by proteoliposomal E180Q-QFR shown in Figure 2 A were fitted to linear and exponential equations (in Tab SII). Three phases are resolved. The first phase is a linear phase corresponding to normal Michaelis-Menten behaviour. The stoichiometry of $MMANH_2$ oxidation relative to H^+ release into the proteoliposomal interior, as calculated from the rate constants in this phase is 2.0 (Table SII). The second phase, an exponential phase, could be caused by a combination of increased $\Delta\mu_{H^+}$ and the accumulation of the first product, MMAN, causing product inhibition after conversion of approximately 8 µmol of $MMANH_2$. This latter effect can also be observed in Figure S3 as determined for the oxidation of $DMNH_2$ by fumarate as catalysed by proteoliposomal E180Q-QFR in presence of the protonophore CCCP, but, also in this case, the net reaction stops after conversion of app. 9 µmol $DMNH_2$. Then, a second linear phase is established, which is attributed to a new steady state of the protonation of the MMAN to $MMANH^+$, resulting in a decrease of the MMAN signal (see Fig. S5A). This event releases the limitations of the first exponential phase, due to removal of MMAN from the steady-state and the removal of H^+ from the equilibrium. The reaction proceeds as can be observed by the ongoing proton release into the proteolipome interior, however at one fifth of the initial rate. No protonation of DMN, the product of the reaction shown in Figure 1D, was observed. The oxidation of $DMNH_2$ by fumarate as

catalysed by proteoliposomal E180Q-QFR in sealed vesicles no longer proceeds significantly after a limited number of turnovers.

We attempted to measure the reversal of the initial pyranine signal after addition of the protonophore CCCP. This was not possible to show in the experiment shown in Figures 2 A and B, due to the strong absorbance of CCCP at the reference wavelength of 415 nm (Fig. S9A). In order to avoid any contribution from CCCP, we chose to monitor the acidification at a wavelength in the open optical window above 450 nm. Fluorescence measurements on proteoliposomal E180Q where performed at the same conditions as in Figures 2 A and B, though excitation wavelength was set to 470 nm and emission wavelength was set to 510 nm (Fig. S9B), where only little optical contributions from the reaction mixture are present . We calibrated the ΔpH-dependent fluorescence in proteoliposomes (Fig. S9 C, D), but we can state the extent of ΔpH only qualitatively due to the absorbance of MMAN at 470 nm (see Figure S5 A) which causes an inner filtering effect which is dependent on the redox ratio. In this experiment we could demonstrate that the addition of the uncoupler CCCP releases the generated ΔpH (Fig. S9E). Although the fluorescence method is highly sensitive, it bears several disadvantages. For instance, an intrinsic calibration with respect to the specific activity of the enzyme is not possible, because these measurements cannot be carried out simultaneously to the monitoring of the quinol oxidation. In addition, its high sensitivity can be disturbed by chromophores absorbing at the excitation or emission wavelengths.

In Figure 2 C the E180Q QFR was not fully inhibited by 20 μM DHN (86.6% inhibition), due to a different experimental geometry. DHN is an amphiphatic compound which is distributed between the aqueous buffer solution and lipophilic liposomal phase. By increasing the volume of the aqueous phase, the effective DHN concentration in the liposome is decreased.

5. Supplementary References

Boyle PH, O´Mahony MJ, Cardin CJ (1984) Reaction of 2-Methyl-1,4-naphthoquinone and its 3-substitued derivatives with active methylene group anions and with diazo compounds. *J Chem Soc Perkin Trans I* **1984:** 593-601

Nicholas KB, Nicholas HB Jr, Deerfield DW II (1997) GeneDoc: Analysis and visualization of genetic variation, *EMBNEW.NEWS* **4:** 14

Notredame C, Higgins DG, Heringa J (2000) T-coffee: a novel method for fast and accurate multiple sequence alignment. *J Mol Biol* **302:** 205-217

Ohta S, Hinata Y, Kawasaki I, Yamashita M (1994) Photo-oxidation of 2-methylamino-3-(1-piperidynyl)-1,4-naphtoquinone. *Chem Pharm Bull* **42:** 2360-2362

Wurm G, Geres U (1984) Untersuchungen an 1,4-Naphthochinonen,7.Mitt. C-Methylierung von 1,4-Naphthochinonen. *Arch Pharm* **317:** 606-609